# Technical Report to the Paper Traction Control Allocation Employing Vehicle Motion Feedback Controller for Four-wheel-independent-drive Vehicle

David Vosahlik, Tomas Hanis

***Abstract*—The technical report contains a deeper analysis and more simulation results for the proposed control architecture solving the control allocation problem. The technical report also contains the parameters of the Matlab & Simulink, and the IPG CarMaker model. The proposed control architecture performance and analysis are shown using high-fidelity FEE CTU in Prague EFORCE formula model implemented in the IPG CarMaker environment with selected test scenarios and compared to the state-of-the-art optimization-based approach.**

***Index Terms*—Vehicle Traction Control, Traction Control Allocation, four-wheel-independent-drive, Vehicle Dynamics Control, Twin-track Vehicle Model**

## I. Introduction

This document extends the Simulation and Results section from the "Traction Control Allocation utilizing Vehicle Motion Feedback Controller for Four-wheel-independent-drive Vehicle" paper. The paper presents a novel traction control allocation scheme based on a vehicle-level motion feedback controller. The paper shows only a limited number of experiments. Therefore, this accompanying technical report presents a deeper analysis, performance evaluation, and further comparison to the state-of-the-art optimization-based solution [1]. A video showing the comparison discussed in the technical report and the accompanying paper is available at [2].

## II. Vehicle Models

The selected parameters of both models, the Matlab & Simulink-based model and the CarMaker model, are presented in this section. The model parameters are shown in the Table I. The simplified Pacejka magic formula parameters are shown in the Table II.

The traction ellipse implementation used in the MATLAB & Simulink model is recapitulated here from [3], [4]. The traction ellipse is introduced to bind the longitudinal and lateral wheel traction capacity. The traction ellipse represents the bounded friction force generated by tire-to-road contact patch, namely, in combined longitudinal and lateral motion. Combined slip occurs when the vehicle is accelerating or braking in a cornering maneuver. A tire cannot generate a combined traction force (comprising of lateral and longitudinal components) greater than the $F_z^{w_i} \cdot \mu_i$, where the $F_z^{w_i}$ is the normal force. That restriction is expressed by the friction ellipse (also called Kamm's circle):

$$F_{combined}^{w_i} = \sqrt{\frac{\left(F_x^{w_i}\right)^2}{\left(\mu_i D_x\right)^2} + \frac{\left(F_y^{w_i}\right)^2}{\left(\mu_i D_y\right)^2}} \leq \mu_i F_z^{w_i}, \tag{1}$$

where $D_x$ and $D_y$ are longitudinal and lateral $D$ Pacejka magic formula parameters.

Let us call the forces calculated using Pacejka Magic formula as $F_{x,max}$ and $F_{y,max}$. Then the following algorithm (Eq. (2) - (6)) is applied to scale (if it is needed) the resulting force:

$$\beta = \arccos\left(\frac{|\lambda|}{\sqrt{\lambda^2 + \sin^2(\alpha)}}\right), \tag{2}$$

$$\mu_{x,act} = \frac{F_{x,max}}{F_z}, \qquad \mu_{y,act} = \frac{F_{y,max}}{F_z}, \tag{3}$$

$$\mu_{x,max} = D_x, \qquad \mu_{y,max} = D_y, \tag{4}$$

$$\mu_x = \frac{1}{\sqrt{\left(\frac{1}{\mu_{x,act}}\right)^2 + \left(\frac{\tan(\beta)}{\mu_{y,max}}\right)^2}}, \qquad F_x = |\frac{\mu_x}{\mu_{x,act}}|F_{x,max}, \tag{5}$$

$$\mu_y = \frac{\tan(\beta)}{\sqrt{\left(\frac{1}{\mu_{x,max}}\right)^2 + \left(\frac{\tan(\beta)}{\mu_{y,act}}\right)^2}}, \qquad F_y = \left|\frac{\mu_y}{\mu_{y,act}}\right| F_{y,max}. \tag{6}$$

TABLE I: Selected parameters of the models.

| Parameter | CarMaker | Simulink |
|---|---|---|
| Nominal wheel radius $[m]$ | 0.205 | 0.33 |
| Vehicle mass $[kg]$ | 155.5 | 1300 |
| Max Front Motors power $[kW]$ | 8 | 150 |
| Max Rear Motors power $[kW]$ | 35 | 200 |
| Distance from CG to rear wheels $[m]$ | 0.83 | 1.63 |
| Distance from CG to front wheels $[m]$ | 1.18 | 1.74 |

TABLE II: Pacejka parameters of the models.

| Model | B | C | D | E |
|---|---|---|---|---|
| CarMaker model | 0.1 | 1.8 | 1 | -0.95 |
| Simulink model | 7 | 1.6 | 1 | -0.5 |

D. Vosahlik is with the Department of Control Engineering, Faculty of Electrical Engineering, Czech Technical University in Prague, Czech Republic. Email: vosahda1@fel.cvut.cz

T. Hanis is with the Department of Control Engineering, Faculty of Electrical Engineering, Czech Technical University in Prague, Czech Republic. Email: hanistom@fel.cvut.cz

D. Vosahlik was supported by the Grant Agency of the CTU in Prague, grant No. SGS19/174/OHK3/3T/13.

The work of Tomas Hanis was supported by the Grant Agency of the CTU in Prague, grant No. GA19-18424S.

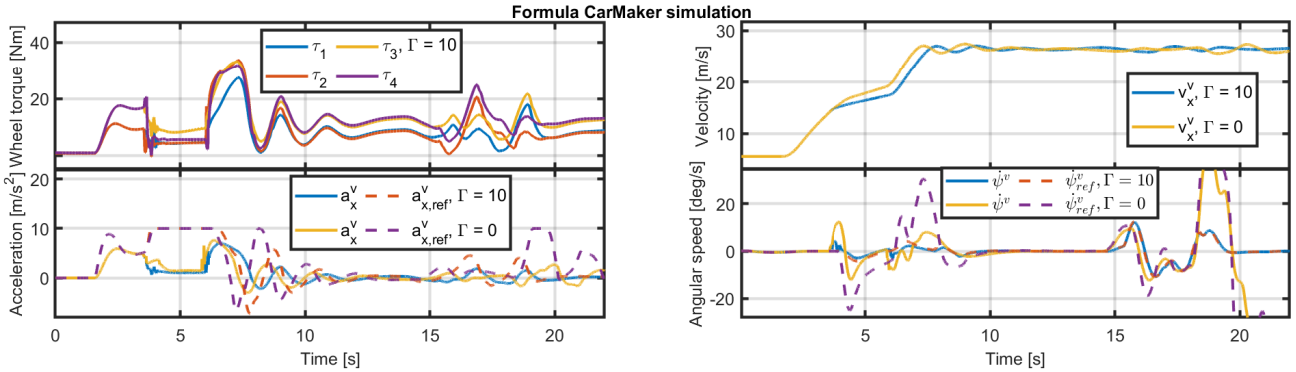


Fig. 1: Comparison of two lateral preference $\Gamma$ values for the CarMaker experiment described in Section III-A1. The figures are from left to right in the first row: wheel torques and vehicle velocity. Next, in the second row: vehicle acceleration with its reference and vehicle yaw rate with its reference. This figure is repeated from the accompanying paper.

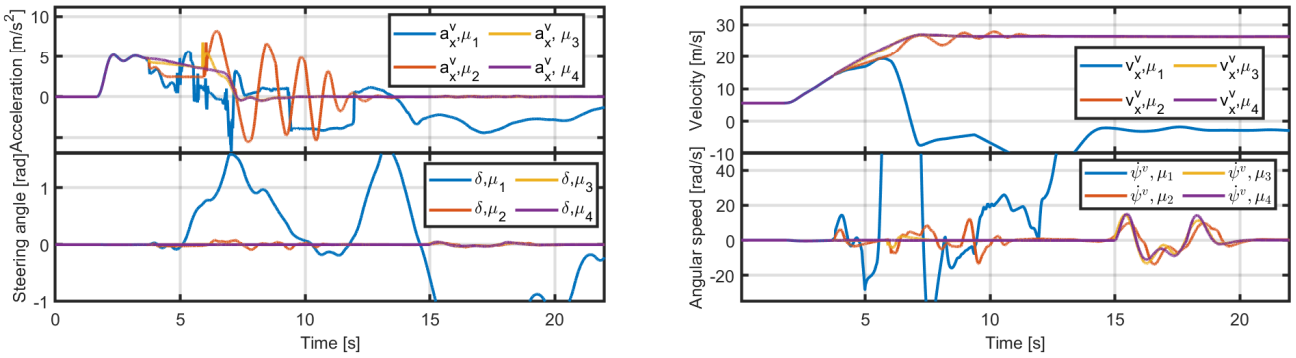


Fig. 2: Comparison of the optimization-based solution [1] for various friction coefficients $\mu_i$ of the friction bump, which is driven over with left side wheels when the vehicle accelerates. Details are explained in Section III-A2.

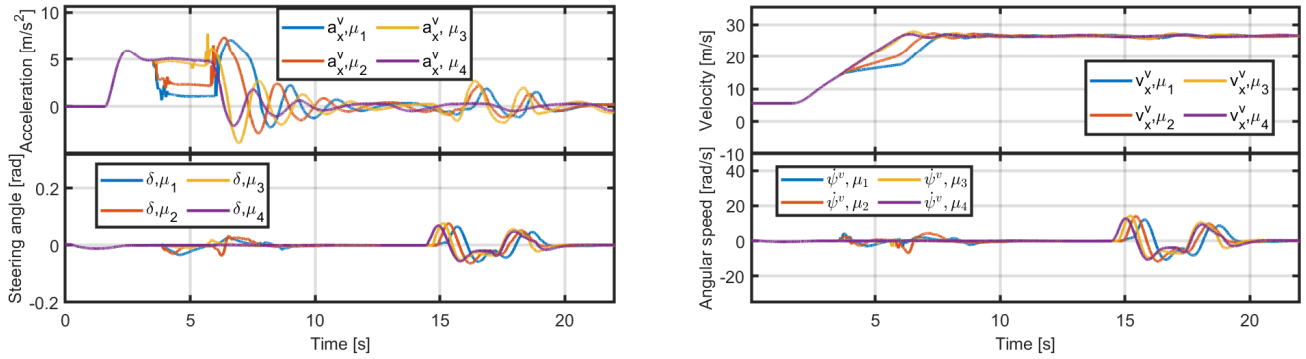


Fig. 3: Comparison of the proposed control system from the accompanying paper for various friction coefficients $\mu_i$ of the friction bump, which is driven over with left side wheels when the vehicle accelerates. Details are explained in Section III-A2.

## III. Extended Experiments

The functionality and performance of the proposed hierarchical control system were validated in the IPG CarMaker environment with high-fidelity FEE CTU in the Prague EFORCE student formula model. A student formula (see Fig. 9) IPG CarMaker validation model is accessible at [5]. The nomenclature is the same as in the accompanying paper. The Pacejka magic formula measured values, which are used in the CarMaker model, are shown in Fig. 10

The calibrated CarMaker formula model with real parameters was used for validation. The drive-by-human controller hierarchy was used in the experiment (see accompanying paper for details).

Two types of experiments were performed to show the controller's performance. The first one is the same as presented in the accompanying paper. Its description is repeated here again for the sake of clarity.

### A. Acceleration and double lane change maneuver

The IPG driver model generates references for the discussed control system via the pedals – an accelerator and a brake pedal. The pedals' positions were translated to vehicle acceleration reference $a^v_{x\ \mathrm{ref}}$. The driver also controls the steering wheel angle $\delta$ translated to vehicle yaw rate reference $\dot{\psi}^v_{\mathrm{ref}}$.

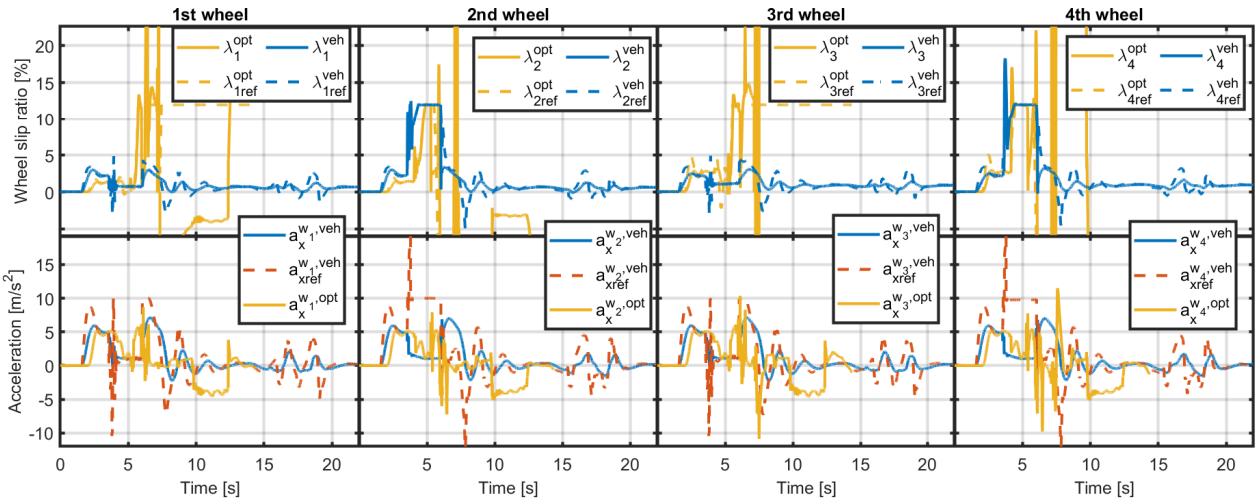


Fig. 4: Wheels acceleration $a_x^{w_i}$ and slip ratio $\lambda_i$ tracking comparison of the proposed allocation scheme (veh superscript is used) and the optimization-based allocation scheme from [1] (opt superscript is used) for the lowest friction coefficient $\mu_1 = 0.15$. Details are described in Section III-A2.

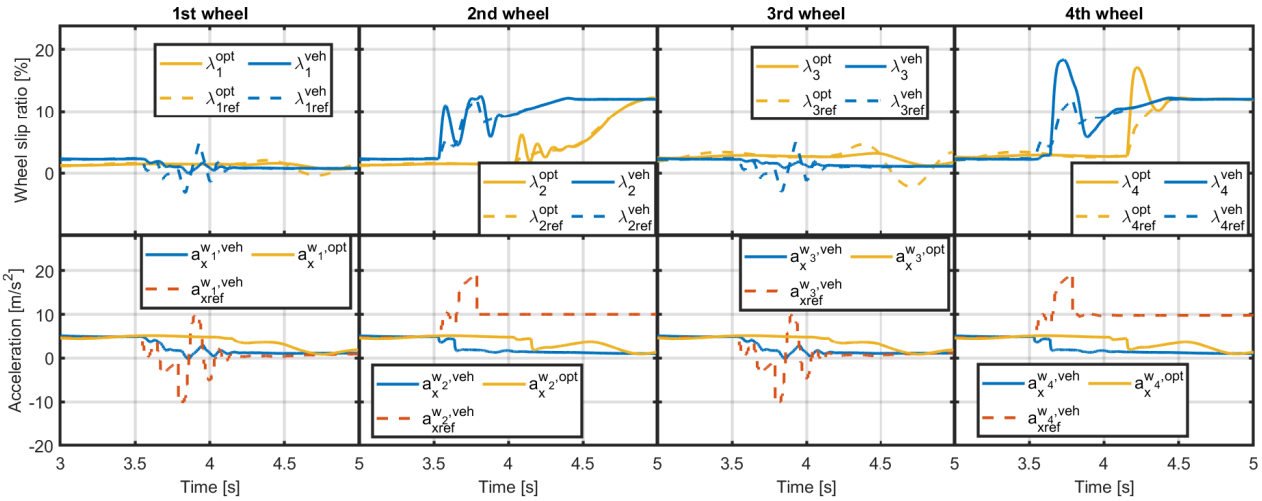


Fig. 5: Detail comparison of the proposed allocation scheme (veh superscript is used) and the optimization-based allocation scheme from [1] (opt superscript is used) is shown in this figure. Wheels' variables ($a_x^{w_i}$, and $\lambda_i$ for each wheel) are shown here for the friction bump's lowest friction coefficient $\mu_1 = 0.15$. Details are described in Section III-A2.

The experiment consists of two parts – acceleration and an ISO 3888-1 double lane change maneuver illustrated in the Fig. 8. The experiment starts with the vehicle maintaining a velocity of 20 km/h. Then, in time $t \approx 2s$ starts the vehicle acceleration. During the acceleration, the vehicle goes over a friction bump ($\mu$ = 0.15) with the left side wheels (approximately $t \in (4, 6)$). Finally, when reaching 95 km/h, an ISO double lane change maneuver is performed (approximately $t \in (15, 20)$).

*1) Lateral preference $\Gamma$ variable comparison:* Lateral preference value $\Gamma$ was presented in the accompanying paper. Please refer to it for further details. The experiment definition is explained in Section II. The difference between two different lateral preference values $\Gamma \in 0, 10$ is shown in the Fig. 1. It can be seen that the different lateral preference values affect the first part of the experiment, where the formula drives through the friction bump. However, the formula maintained lateral stability. In contrast, the double lane change is not possible with $\Gamma = 0$ at such high speed (vehicle velocity $v_x^v = 95km/h$).

*2) Varying friction bump friction comparison:* Varying friction coefficient value $\mu_i \in \{0.15, 0.25, 0.4, 0.8\}$ of the friction bump, which is driven over during acceleration, is discussed in this section. The experiment definition is explained in Section II.

First, the optimization-based solution [1] is compared for all the friction coefficient variations in the Fig. 2. With the optimization-based solution, the driver could not go over the lowest friction surface $\mu_1 = 0.15$. Various reasons could be the root cause of this behavior. The IPG driver is counteracting the yaw rate disturbance caused by a different surface on the left side wheels, which can be the source of the oscillations –

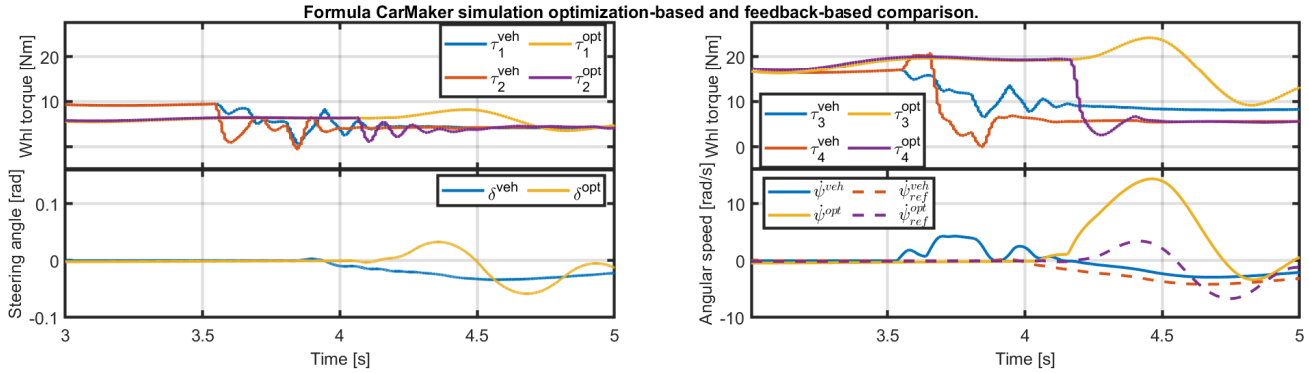


Fig. 6: Detail comparison of the proposed allocation scheme (veh superscript is used) and the optimization-based allocation scheme from [1] (opt superscript is used) is shown in this figure. Wheels' torques $\tau_i$, driver's steering wheel command $\delta$, and vehicle yaw rate $\dot{\psi}^v$ are shown here for the friction bump lowest friction coefficient $\mu_1 = 0.15$. Details are described in Section III-A2.

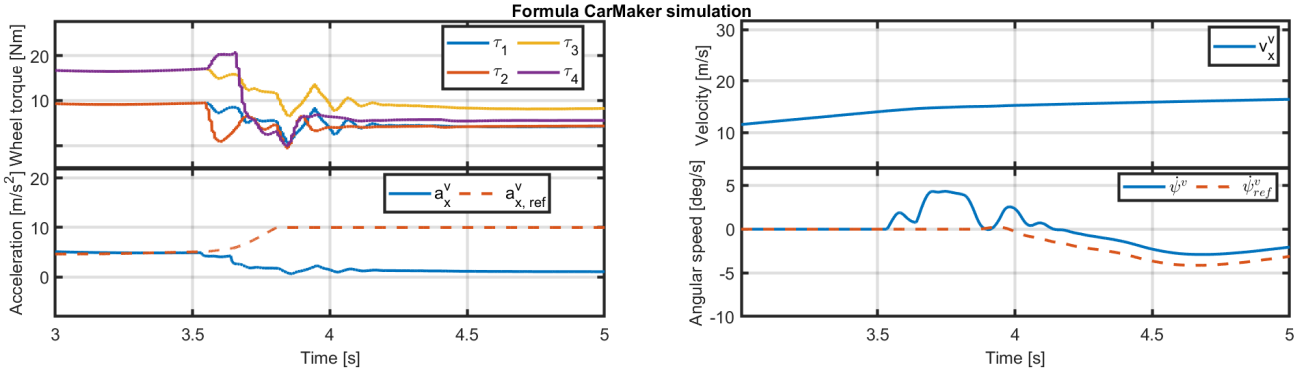


Fig. 7: Detail of the proposed allocation scheme is shown in this figure. Wheels' torques $\tau_i$, vehicle yaw rate $\dot{\psi}^v$, vehicle acceleration $a_x^v$, and vehicle velocity $v_x^v$ are shown here for the friction bump lowest friction coefficient $\mu_1 = 0.15$. Details are described in Section III-A2.

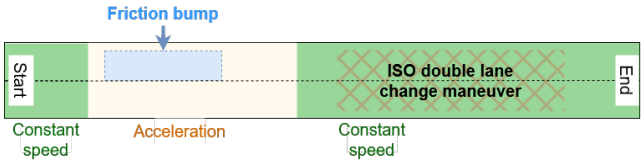


Fig. 8: Acceleration and double lane change maneuver containing the friction bump used in the Section II.

Fig. 9: EFORCE student formula used for CarMaker model.

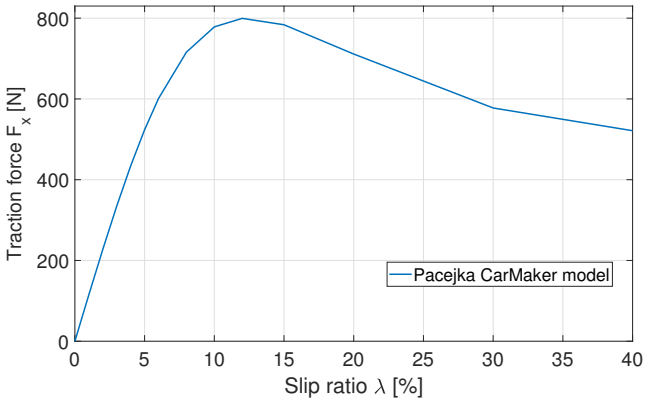


Fig. 10: Slip curve used in the CarMaker model. It is implemented using Pacejka magic formula, fitted on the measured values.

driver-induced oscillation. Next, the left-side wheels cannot deliver the required force due to traction limits, which is not handled in the optimization-based solution. Finally, the optimization-based solution is tracking yaw rate reference $\dot{\psi}^v_{\text{ref}}$ only in an open loop manner (no feedback is present). The yaw rate reference is transformed into the required vehicle body torque $M_z$ that is then used to calculate individual wheels force reference as described in [1].

Next, the same comparison for all the surface types of the

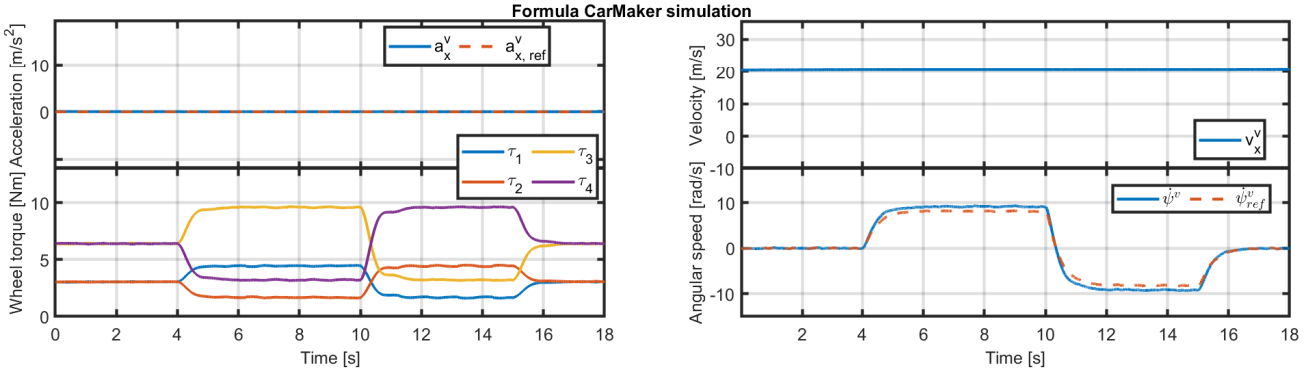


Fig. 11: Torque vectoring experiment described in Section III-B. The optimization-based control allocation proposed in [1] performance is shown in this figure. Vehicle acceleration $a_x^v$, velocity $v_x^v$, yaw rate $\dot{\psi}^v$ and wheel torques $\tau_i;\ i \in 1,2,3,4$.

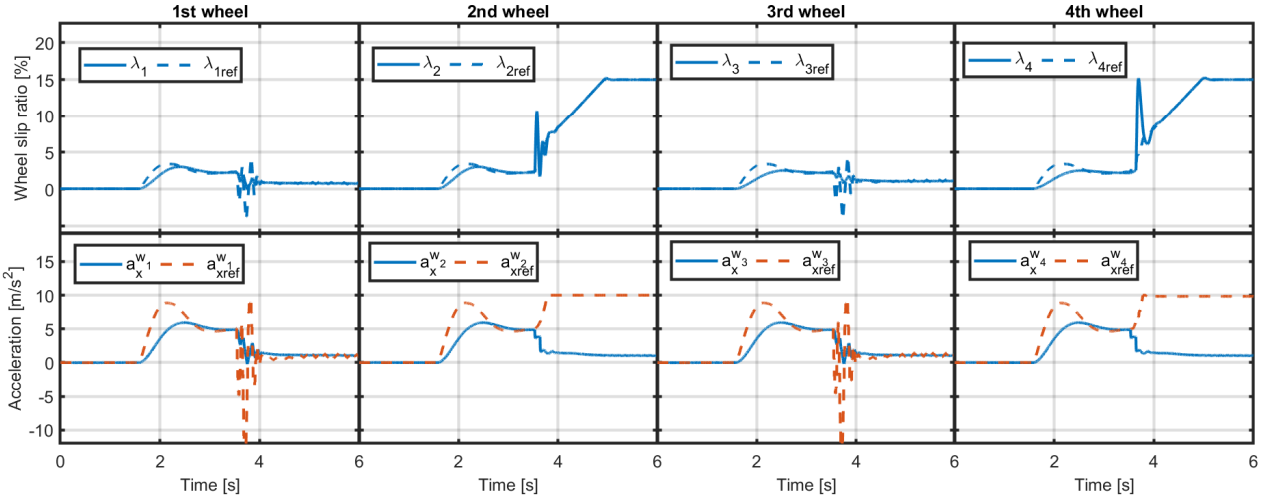


Fig. 12: Detail of the proposed allocation scheme is shown in this figure. Wheels' variables ($a_x^{w_i}$, and $\lambda_i$ for each wheel) are shown here for the friction bump's lowest friction coefficient $\mu_1 = 0.15$. The maximum slip ratio $\lambda_{\max}$ was set to 15% simulating wrong $\lambda_{\max}$ parameter estimation. Details are described in Section III-A3.

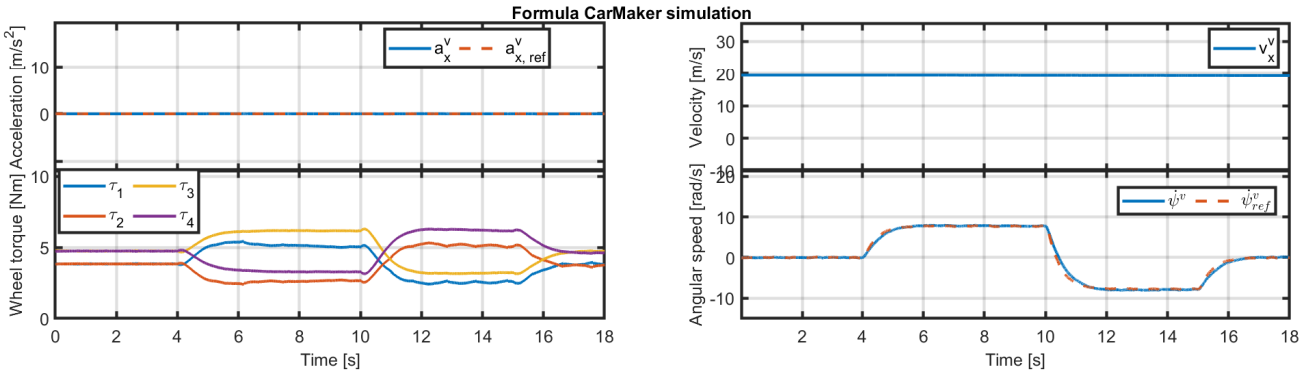


Fig. 13: Torque vectoring experiment described in Section III-B. The proposed control allocation performance is shown in this figure. Vehicle acceleration $a_x^v$, velocity $v_x^v$, yaw rate $\dot{\psi}^v$ and wheel torques $\tau_i;\ i \in 1,2,3,4$.

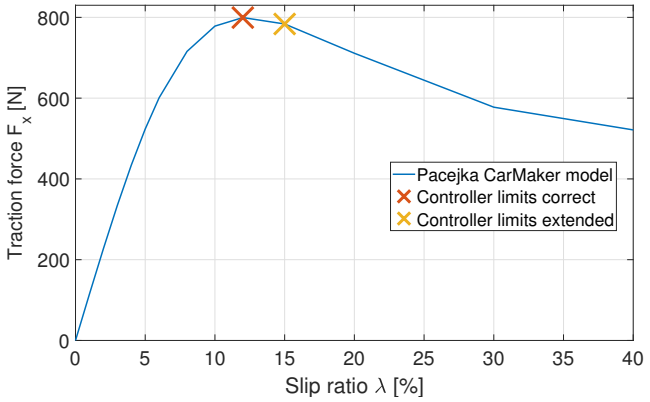


Fig. 14: Pacejka magic formula measured values used in the CarMaker model. The limit value used as $\lambda_{\max}$ value in the control system is selected once correctly and once extended behind the true $\lambda_{\max}$ to simulate wrong $\lambda_{\max}$ estimation.

control system proposed in the accompanying paper is shown in Fig. 3. The driver could handle all the friction coefficient values using the control system proposed in the accompanying paper compared to the case when the driver was using the optimization-based solution [1] shown in the Fig. 2. The proposed control system in the accompanying paper introduces vehicle-level motion feedback control law, ensuring the correct vehicle reference tracking even in extreme conditions.

The comparison for the lowest friction coefficient $\mu_1$ of both optimization-based and the proposed solution from the accompanying paper, on the wheel level, is shown in the Fig. 4. A detail of the moment when the vehicle enters the friction bump is shown in the Figures 5 and 6. The proposed control system's details from the accompanying paper are shown in the Fig. 7. It can be seen that the optimization-based system from [1] works well while driving the nominal surface. The disturbance in yaw rate tracking is significant once the vehicle enters the low friction surface with the left wheels. This is not the case for the proposed system, where the traction limits are respected. The second and fourth wheel applies a maximum slip ratio, which is still insufficient to track the requested vehicle acceleration (see Fig. 5). The vehicle acceleration reference tracking is impossible due to physical constraints on the friction bump. Therefore, the proposed system from the accompanying paper goes with the highest possible acceleration that still tracks the yaw rate reference provided by the driver turning the steering wheel. This can be especially seen in the Fig. 7. The disturbance rejection of the proposed system from the accompanying paper is much better than the optimization-based solution of [1].

*3) Inaccurate $\lambda_{max}$ estimate:* The Pacejka magic formula slip curve used in the IPG CarMaker model is shown in the Fig. 10. The control system proposed was tuned for the stable region of the slip curve, where $|\lambda| < \lambda_{\max} = 12\%$ (see Fig. 14). However, estimating the $\lambda_{\max}$ parameter is a demanding task. Thus, the $\lambda_{\max}$ could eventually be inaccurately estimated. An experiment simulating an inaccurate $\lambda_{\max}$ estimate is presented in this section. The controller limit $\lambda_{\max}$ was in this experiment set up to the inaccurate value $\lambda_{\max} = 15\%$, which is already behind the slip curve maximum in the unstable region (see Fig. 14). According to local linearization analysis in this operating point, the controlled system is still stable (see the accompanying paper). The performance of the system for wrong estimated $\lambda_{\max}$ is shown in the Fig. 12. It can be seen that the system tracks well even the slip ratio values already from the unstable slip curve region.

### B. Lateral stability functionality

The second experiment shows the vehicle yaw rate tracking capability of the proposed control system from the accompanying paper using the wheel torques. One can understand this as a torque vectoring functionality. The wheels are not steered in any way ($\delta_1 = \delta_2 = 0$) to show the steering capability of the proposed solution. The proposed system based on the vehicle motion feedback controller's performance is shown in the Fig. 13. For comparison, the optimization-based solution torque vectoring is shown in Fig. 11. It can be seen that both systems can track requested yaw rate references quite well.

## IV. Conclusion

Results extending the experiments section of the accompanying paper Traction Control Allocation utilizing Vehicle Motion Feedback Controller for Four-wheel-independent-drive Vehicle was presented here. The proposed and state-of-the-art optimization-based solution [1] were compared for various friction bump coefficients representing dry asphalt, wet asphalt, snow, and ice (see Section III-A). Next, robustness to the inaccurate $\lambda_{max}$ estimate is shown in the Section III-A3. Finally, the lateral stability is discussed in the Section III-B.

## References

[1] K. Maeda, H. Fujimoto, and Y. Hori, "Four-wheel driving-force distribution method for instantaneous or split slippery roads for electric vehicle with in-wheel motors," *International Workshop on Advanced Motion Control, AMC*, 2012.

[2] Smart Driving Solutions Research Center, "SDS youtube," 2022. [Online]. Available: https://www.youtube.com/watch?v=9BoSNcziuhw

[3] D. Efremov, T. Hanis, and M. Hromcik, "Introduction of Driving Envelope and Full-Time-Full-Authority Control for Vehicle Stabilization Systems," in *2019 22nd International Conference on Process Control (PC19)*. IEEE, jun 2019, pp. 173–178. [Online]. Available: https://ieeexplore.ieee.org/document/8815305/

[4] Adams/Tire. Using the PAC2002Tire Model. [Online]. Available: https://docplayer.net/54206752-Using-the-pac2002tire-model.html

[5] Smart Driving Solutions Research Center, "SDS github," 2022. [Online]. Available: https://github.com/SDS-RC-FEE-CTU-in-Prague/TwinTrack